

Effects of fluctuating daily surface fluxes on the time-mean oceanic circulation

Article

Accepted Version

Balan Sarojini, B. and Von Storch, J.-S. (2009) Effects of fluctuating daily surface fluxes on the time-mean oceanic circulation. *Climate Dynamics*, 33 (1). pp. 1-18. ISSN 0930-7575 doi: <https://doi.org/10.1007/s00382-009-0575-y> Available at <https://centaur.reading.ac.uk/5886/>

It is advisable to refer to the publisher's version if you intend to cite from the work. See [Guidance on citing](#).

Published version at: <http://www.springerlink.com/content/65857m37010658II/>

To link to this article DOI: <http://dx.doi.org/DOI:10.1007/s00382-009-0575-y>

Publisher: Springer

Publisher statement: The original publication is available at www.springerlink.com

All outputs in CentAUR are protected by Intellectual Property Rights law, including copyright law. Copyright and IPR is retained by the creators or other copyright holders. Terms and conditions for use of this material are defined in the [End User Agreement](#).

www.reading.ac.uk/centaur

CentAUR

Central Archive at the University of Reading

Reading's research outputs online

Effects of fluctuating daily surface fluxes on the
time-mean oceanic circulation

†Balan Sarojini Beena and Jin-Song von Storch

Max-Planck Institute for Meteorology, Hamburg, Germany

March 28, 2009

revised version to *Climate Dynamics*

Corresponding author: Jin-Song von Storch

Max-Planck Institute for Meteorology

Bundestrasse 53, 20146 Hamburg, Germany

Phone: +49 40 41173 155, Fax: +49 40 41173 366

Email: jin-song.von.storch@zmaw.de

[†]Present address: National Centre for Atmospheric Science - Climate,
Walker Institute for Climate System Research, Department of Meteorology
University of Reading, Reading RG6 6BB, United Kingdom

Abstract

The effect of fluctuating daily surface fluxes on the time-mean oceanic circulation is studied using an empirical flux model. The model produces fluctuating fluxes resulting from atmospheric variability and includes oceanic feedbacks on the fluxes. Numerical experiments were carried out by driving an ocean general circulation model with three different versions of the empirical model. It is found that fluctuating daily fluxes lead to an increase in the Meridional Overturning Circulation (MOC) of the Atlantic of about 1 Sv and a decrease in the Antarctic Circumpolar Current (ACC) of about 32 Sv. The changes are approximately 7% of the MOC and 16% of the ACC obtained without fluctuating daily fluxes.

The fluctuating fluxes change the intensity and the depth of vertical mixing. This, in turn, changes the density field and thus the circulation. Fluctuating buoyancy fluxes change the vertical mixing in a non-linear way: They tend to increase the convective mixing in mostly stable regions and to decrease the convective mixing in mostly unstable regions. The ACC changes are related to the enhanced mixing in the subtropical and the mid-latitude Southern Ocean and reduced mixing in the high-latitude Southern Ocean. The enhanced mixing is related to an increase in the frequency and the depth of convective events. As these events bring more dense water downward, the mixing changes lead to a reduction in meridional gradient of the depth-integrated density in the Southern Ocean and hence the strength of the ACC. The MOC changes are related to more subtle density changes. It is found that the vertical mixing in a latitudinal strip in the northern North Atlantic is more strongly enhanced due to fluctuating fluxes than the mixing in a latitudinal strip in the South Atlantic.

40 This leads to an increase in the density difference between the two strips, which
41 can be responsible for the increase in the Atlantic MOC.

42 Keywords : Fluctuating daily fluxes, Vertical mixing, Meridional Overturning Cir-
43 culation, Antarctic Circumpolar Current, Air-Sea interaction.

1 Introduction

The issue of what determines the strength of the global Meridional Overturning Circulation (MOC) has drawn the attention of many researchers. The prevailing view is that the circulation is driven partly by the diapycnal mixing of heat that lightens water masses in the deep ocean and causes them to rise uniformly in low latitudes (Munk and Wunsch 1998), and partly by wind-driven upwelling induced by the strong westerly circumpolar winds in the Southern Ocean (Webb and Suginohara 2001, Toggweiler and Samuels 1995). Both the diapycnal mixing and the wind-driven upwelling focus on the mechanisms that allow deep dense water masses to return to the surface. The surface buoyancy forcing, though not considered as a driver of the MOC capable for providing energy supply, is necessary for setting up the flow by controlling the rate and site of the deep water formation (Kuhlbrodt et al. 2007).

The major factors which control the MOC in the above picture are the diapycnal mixing, the upwelling due to wind forcing and the rate and the site of deep water formation set up by the surface buoyancy forcing. All these factors are directly or indirectly related to the air-sea fluxes. So far, the analyses have mainly focused on the effects of *climatological mean* components of the wind forcing in providing the energy required for diapycnal mixing or in inducing wind-driven upwelling (Munk and Wunsch 1998, Webb and Suginohara 2001, Toggweiler and Samuels 1995). This paper aims at a detailed picture that can isolate the effect of *fluctuating day-to-day fluxes* from that of the mean fluxes.

Generally, the role of air-sea fluxes in determining the stratification and the circu-

66 lation of the oceans has been known for long time. Such a role has been investigated
67 within theoretical frameworks (Walín 1982 and Tziperman 1986) and with respect to
68 change in convection (Rahmstorf 1995, Kuhlbrodt and Monahan 2003, Swingedouw
69 et al. 2007). Walín (1982) studied the relation between sea-surface heat flux and
70 thermal circulation in the ocean. Tziperman (1986) derived a relation between the
71 interior stratification and the air-sea heat fluxes and used this relation to study the
72 buoyancy driven circulation. The role of surface flux anomalies in triggering convec-
73 tion was studied by Rahmstorf (1995). Using a simple box model, Kuhlbrodt and
74 Monahan (2003) showed that the variability of surface fluxes is important for the
75 open ocean convection and deep water formation in the Labrador Sea. Swingedouw
76 et al. (2007) found a linear relationship between density changes in the convection
77 sites and the strength of the Atlantic MOC.

78 Even though the previous studies support the important role of day-to-day
79 anomalies of air-sea fluxes, it is generally difficult to obtain a quantitative esti-
80 mation of the impact of all fluctuating fluxes on the MOC in the framework of
81 GCMs. For instance, it is obvious that an evaporation anomaly can lead to the
82 formation of water denser than 1028 kg/m^3 , while a precipitation anomaly can lead
83 to the formation of water lighter than 1028 kg/m^3 . With these anomalies, water
84 mass production denser than 1028 kg/m^3 can occur. Without these anomalies, but
85 with the same time-mean buoyancy forcing, the water mass production denser than
86 1028 kg/m^3 would have been zero. However, what is less clear is the net effect of all
87 buoyancy anomalies on the oceanic circulation.

88 The effect of fluctuating fluxes can be strongly non-linear. For example, consider
89 buoyancy anomalies occurring in a mostly stable region. In this case, positive anoma-
90 lies (e.g. due to a precipitation event or a downward positive heat flux anomaly) may
91 not significantly affect the statistics of convective events (since the water column is
92 already stable), whereas negative anomalies (e.g. due to an evaporation event or a
93 negative heat flux anomaly) could significantly increase convective events, resulting
94 in non-linear responses to fluctuating fluxes.

95 Given the potential and complexity of daily air-sea fluxes in changing the water
96 mass production and from that the interior stratification and circulation, the effect
97 of daily fluxes is investigated using a coupled system, specially developed for this
98 purpose. The system consists of an ocean GCM and an empirical global flux model
99 which describes the day-to-day flux variations in a realistic manner. The advantage
100 of this system is that it allows a separation of effects of fluctuating air-sea fluxes
101 from that of the climatological mean fluxes. Such a separation is difficult within a
102 fully coupled atmosphere and ocean GCM. Numerical experiments were carried out
103 using the hybrid coupled model. As will be shown, the fluctuating daily fluxes affect
104 not only the Atlantic MOC, but also the Antarctic Circumpolar Current (ACC).
105 The models and the numerical experiments are described in Section 2 and 3. The
106 results of the experiments are presented in Section 4. Discussion and conclusions
107 are given in the final section.

2 Model Description

The empirical flux model and the OGCM used in this study are briefly introduced below. A more detailed description can be found in von Storch et al. (2005) and Marsland et al. (2003).

2.1 The empirical model of daily air-sea fluxes: EMAD

The flux model, referred to as EMAD (Empirical Model of Atmospheric Dynamics), is designed to generate air-sea flux anomalies relative to given climatological mean fluxes. Based on the assumption that deviations from a given mean state of the coupled system are small, the dynamics of the flux anomalies and the response of these fluxes to anomalous sea surface condition are considered to be linear and described by

$$\mathbf{x}'_{t+1} = \mathcal{A}\mathbf{x}'_t + \mathcal{C}\mathbf{n}_{t+1} + \mathcal{B}\mathbf{y}'_t. \quad (1)$$

\mathbf{x}' comprises anomalies of all fluxes required to drive the OGCM. These are the net heat flux, the zonal and meridional momentum flux, the freshwater flux, the short-wave radiation which penetrates into the sea water, and the conductive and residual heat flux required to describe the sea ice formation and depletion. \mathbf{y}' represents anomalies of oceanic variables at the sea surface, such as the SST, the sea ice cover and the sea ice thickness, that can affect the fluxes. \mathbf{n} is a multivariate white noise with zero mean and unit variance. \mathcal{A} describes the linear dynamics of the fluxes, \mathcal{B} the linear response of fluxes to the ocean surface condition, and \mathcal{C} the covariance structure of the residual that is not depicted by \mathcal{A} and \mathcal{B} . The time step of Eq.(1)

128 is one day.

129 \mathcal{A} , \mathcal{B} and \mathcal{C} are matrices obtained by fitting Eq.(1) on to the daily output of a
130 200-year control integration performed with the fully coupled ECHO-G Atmosphere
131 Ocean General Circulation Model (AOGCM) (Legutke and Voss 1999 ; Raible et
132 al. 2001). The fitting is done first for \mathcal{A} and \mathcal{B} in EOF-spaces represented by the
133 leading EOFs of fluxes and then for \mathcal{C} in the physical space. We use 100 EOFs for
134 each flux and 100 EOFs for SST in the water module (further explained below) and
135 50 EOFs for each of the same variables in the ice module. The physical space has
136 the Gaussian grid of T30 resolution.

137 The EMAD model consists of a water module and an ice module for the separate
138 treatment of the fluxes over permanently open water and sea surface where ice can be
139 formed. The formulation of the two modules is necessary to deal with the additional
140 fluxes which are required to drive the sea-ice model. Different from the water module,
141 the state vector \mathbf{x}' in the ice module contains the conductive and residual heat and
142 distinguishes the fluxes of net heat, fresh water and momentum over ice and water.
143 Depending on the sea ice fraction within a grid cell, either the fluxes over ice or the
144 fluxes over water or both will be used to drive the ocean.

145 Without the last term, the model equation (1) mimics the linear dynamics of flux
146 anomalies driven by the atmospheric variability. The last term with \mathcal{B} describes the
147 oceanic feedbacks on the fluxes. Since \mathcal{B} is derived from a coupled model integration
148 which is essentially statistically stationary, the interaction described by $\mathcal{B}\mathbf{y}'$ acts to
149 keep the ocean in the given mean state. This means that, if the sea surface condition

150 is moved away from the given sea surface state, there would be non-zero anomalies
 151 of sea surface variables and from that a non-zero \mathbf{y}' , which generates anomalous
 152 fluxes $\mathcal{B}\mathbf{y}'$ that drive the sea surface back to the given state.

153 The just described feedback mechanism involves essentially the interaction be-
 154 tween the heat flux and the SST anomalies. It functions in a way as if the heat flux
 155 is described by a restoring condition. However, in contrast to the traditional restor-
 156 ing formulation which uses a constant restoration time, \mathcal{B} implies a dependence of
 157 the restoration time on spatial scales. By formulating in EOF-space, \mathcal{B} captures the
 158 restoring time scales for modes with different spatial scales in the ECHO-G integra-
 159 tion. In particular, large-scale SST anomalies are allowed to exist over a longer time
 160 period, while small-scale SST anomalies will be damped out quickly. The need for
 161 such a scale-dependent restoration was first pointed out by Rahmstorf and Wille-
 162 brand (1995). The present formulation can be considered as an empirical approach
 163 that captures the scale-dependent feedback of SST on heat flux in the ECHO-G inte-
 164 gration. Due to the scale dependence, the $\mathcal{B}\mathbf{y}'$ -term does not act as a rigid restoring.
 165 One does not obtain exactly the same SST when using $\mathcal{B}\mathbf{y}'$ to nudge SSTs to the
 166 same climatological mean SST (see Section 4.1).

167 By collecting all fluxes into vector \mathbf{x}' and all relevant sea surface variables in
 168 vector \mathbf{y}' , the model equation (1) ensures that the fluxes and the oceanic variables
 169 are physically coherent. When coupling EMAD to an OGCM, the fluxes of heat,
 170 fresh water and momentum will not respond independently to a given anomalous
 171 state of the sea surface.

172 The noise term acts to excite the EOF-modes described by the deterministic part
 173 of EMAD (i.e. by \mathcal{A} - and \mathcal{B} -terms). The matrix \mathcal{C} ensures that the distributions of
 174 the total variances of the fluxes match those obtained from the coupled ECHO-G
 175 model.

176 Despite the extremely simple form, the model equation (1) is able to describe
 177 various types of air-sea interactions. If $\mathcal{A}\mathbf{x}' + \mathcal{C}\mathbf{n}$ dominates $\mathcal{B}\mathbf{y}'$ for a certain flux,
 178 this flux would force the ocean by and large stochastically. This could be the case
 179 for wind stress anomalies over high-latitudes, where the influence of the SST on
 180 the wind stress is weak. If the \mathcal{A} -term and the \mathcal{B} -term have similar strength, the
 181 flux would be affected both by the stochastic forcing and by the oceanic feedback.
 182 If the \mathcal{B} -term dominates, the flux would be essentially determined by the oceanic
 183 conditions. The relative importance of the various types of air-sea interactions is
 184 given by the amplitudes of elements of \mathcal{A} and \mathcal{B} . The result of different types of
 185 air-sea interactions can be identified by studying the lagged correlation functions
 186 between the flux and SST (Frankignoul et al. 1998 ; von Storch 2000).

187 The ability of EMAD in reproducing the second moments of fluxes found in the
 188 coupled ECHO-G is considered in von Storch et al. (2005). In particular, it was
 189 shown that EMAD produces variances of fluxes, whose strength and distribution are
 190 in general comparable to that found in ECHO-G. The various types of interactions,
 191 as can be identified using the lagged correlation functions between the SST and the
 192 fluxes (Frankignoul et al. 1998 ; von Storch 2000), are by and large reproduced
 193 when coupling EMAD to an OGCM. Finally, EMAD is able to act realistically to

194 anomalous sea surface condition, such as those related to an ENSO event or to a
195 Polynya.

196 To give the reader an idea of how the EMAD-fluxes look like, Figure 1 shows
197 anomalies of wind stress (arrows) and heat flux (colour shading), obtained by forc-
198 ing EMAD with the anomalous sea surface conditions derived from the coupled
199 ECHAM5/MPI-OM AOGCM (Jungclaus et al. 2005). Also shown in Figure 1 is a
200 snapshot of the anomalies of the same fluxes from the NCEP reanalysis for an arbi-
201 trary day. Similar to the fluxes of the reanalysis, the EMAD-fluxes have maxima at
202 the mid- and high-latitudes. The amplitudes of EMAD-anomalies are slightly larger
203 than those of the reanalysis. The structure of the EMAD-anomalies are somewhat
204 smoother than that of the NCEP-fluxes, reflecting the fact that EMAD describes
205 the leading EOF-modes excited by white noise forcing. Figure 1 and the previous
206 validation (von Storch et al. 2005) suggest that EMAD is capable of producing the
207 basic features of the fluctuating day-to-day fluxes.

208 **2.2 The Ocean General Circulation Model: MPI-OM**

209 The OGCM used in this study is the Max-Planck Institute Ocean Model (MPI-
210 OM). It is a z-coordinate model based on primitive equations for a Boussinesq fluid
211 on a rotating sphere. It is formulated on the horizontal Arakawa C grid with the
212 north pole located at northern Greenland and south pole close to Weddell Sea. It
213 has horizontal resolution varying from 20 km in the main sinking regions associated
214 with the MOC to about 350 km in the tropics. For the present study, the model

configuration with 40 vertical levels (Haak et al. 2003) is used. The model contains a free surface and a state-of-the-art sea ice model with viscous-plastic rheology and snow. Overflow over the sills and off continental shelves are represented by a bottom boundary layer slope convection scheme.

Tracer diffusion is isoneutral and dianeutral and is described by the diffusion tensor \mathcal{K} (Redi 1982), which is a function of the neutral density gradient and horizontal and vertical diffusion coefficients K_H and K_V . The scheme is numerically implemented following Griffies (1998). The effect of horizontal tracer mixing by advection due to the unresolved mesoscale eddies is parameterized after Gent et al. (1995). The horizontal eddy viscosity is parameterized using a scale-dependent biharmonic formulation. The vertical eddy viscosity follows Pacanowski and Philander (1981). It utilizes an eddy coefficient which is represented in the same way as the vertical eddy diffusivity coefficient K_V (see Eq.(2) below), except that the Richardson-number dependent part is proportional to $(1 + C_{RD}R_i)^{-2}$, rather than $(1 + C_{RD}R_i)^{-3}$ as given in Eq.(3). The vertical diffusion, as described by K_V or in short K , plays an important role in the present study and is further described below.

K is a function of convective mixing, Richardson number (Ri) dependent mixing, wind-induced mixing and background diffusivity (Marsland et al. 2003) and is given by

$$K = \begin{cases} K_{conv} & \text{if statically unstable} \\ K_{Ri} + K_{wind} + K_{back} & \text{if statically stable} \end{cases} \quad (2)$$

235 with

$$K_{Ri} = D_{VO}(1 + C_{RD}R_i)^{-3}, \quad (3)$$

236 where R_i is the Richardson number, $D_{VO} = 2 \times 10^{-3} \text{ m}^2 \text{ s}^{-1}$ and $C_{RD} = 5$ are model
237 constants. According to Eq.(3), the maximum value of K_{Ri} is $2 \times 10^{-3} \text{ m}^2 \text{ s}^{-1}$. The
238 diffusion related to convection K_{conv} is set to $10^{-1} \text{ m}^2 / \text{s}$. Thus, static instability
239 is removed by switching on an extremely strong mixing. In the surface layer, the
240 wind-induced mixing K_{wind} over ice free regions is given by

$$K_{wind} = W_T V_{10}^3 \quad (4)$$

241 where V_{10} is the local 10 m wind speed and W_T equals $5 \times 10^{-4} \text{ m}^{-1} \text{ s}^2$. Below the
242 surface, K_{wind} depends on the stability of the water column and decays exponentially
243 with e -folding depth being 40 m. The diffusion related to other unresolved processes,
244 such as internal waves, is described by $K_{back} = 10^{-5} \text{ m}^2 / \text{s}$. This set of parameters
245 is used in the integration of MPI-OM coupled to the ECHAM5 AGCM (Jungclaus
246 et al. 2005) that produces a realistic oceanic state.

247 The vertical diffusion coefficient K can vary spatially and temporally, depending
248 on the static stability and wind forcing. Since K_{back} is unchanged in the experiments
249 performed and since K_{wind} is confined to the first 40 meters of the ocean (depending
250 on the stability), the changes in K below 40 meters are related to the changes in
251 K_{Ri} and / or K_{conv} . Fluctuating fluxes can change both K_{Ri} and K_{conv} .

252 Fluctuating fluxes can affect K_{conv} by turning convection on and off in a non-
253 linear way, depending on the background static stability. In the regions where

254 the stratification is mostly stable and K_{conv} is mostly turned off, a positive buoy-
 255 ancy forcing (induced e.g. by additional precipitation events or additional heat flux
 256 anomalies) makes the ocean more stable and hence will leave K_{conv} switched off. By
 257 contrast, a negative buoyancy forcing will reduce static stability, and hence K_{conv}
 258 might be switched on more often. The net effect is an increase in the convective
 259 mixing. Examples of mostly stable oceans are the tropical and subtropical oceans.
 260 On the other hand, in regions where the stratification is mostly unstable and K_{conv}
 261 is mostly switched on, a negative buoyancy forcing will not affect the convective mix-
 262 ing much, since the convective mixing is already switched on. A positive buoyancy
 263 anomaly on the contrary can increase the static stability, making K_{conv} switched on
 264 less often. The net effect is a decrease in K . Examples of mostly unstable oceans
 265 are the GIN (Greenland Iceland Norwegian) Seas and the high-latitude Southern
 266 Ocean in the MPI-OM model.

267 The above described changes in convective events are not inconsistent with pre-
 268 vious numerical experiments in which the convection at single grid points can be
 269 switched on and off by flux anomalies and be crucial for maintaining deep water
 270 formation (Rahmstorf 1995, Kuhlbrodt and Monahan 2003).

271 Fluctuating fluxes can also change the Ri -dependent mixing, since a fluctuating
 272 buoyancy flux can affect the stratification of the water column and a fluctuating wind
 273 stress forcing can alter the shear of the current. The change in the Ri -dependent
 274 mixing is expected to be more pronounced in the tropics. In these regions, the
 275 static stability of the ocean is so high that static instability rarely occurs and, when

276 it occurs, it will be confined to a shallow surface layer.

277 In the present study, the vertical diffusion coefficient K is stored on monthly
278 basis. Since the maximum value of K_{Ri} of $2 \times 10^{-3} \text{ m}^2 \text{ s}^{-1}$ is much smaller than
279 $K_{conv} = 10^{-1} \text{ m}^2 / \text{s}$, large changes in K must be related to changes in the number of
280 convective events occurring within a month. Generally, a large increase (decrease)
281 in K indicates an increase (a decrease) in the number of convective events, and from
282 that an increase (a decrease) in the formation of dense water masses. In this sense,
283 changes in K can be used as a crude measure of changes in water mass formation
284 due to convection. As shown by the mean convection depth in Figure 10a, the true
285 deep water formation, reaching about 1000 meter depth on average, occurs only in
286 GIN seas and off the Antarctic coast in the Atlantic sector in the version of the
287 MPI-OM model used here.

288 **2.3 The Coupled Model: EMAD/MPI-OM**

289 To couple the EMAD with the MPI-OM, the EMAD fluxes, which are on the T30-
290 Gaussian grid, are interpolated into the curvilinear grid of the MPI-OM model. The
291 coupling takes place once a day.

292 When coupling EMAD to the MPI-OM model, one needs a set of fields of climato-
293 logical mean fluxes and a set of fields of climatological mean sea surface conditions.
294 Both sets were derived from the last 50 years of a 600-year integration with the
295 ECHAM5/MPI-OM coupled AOGCM (Jungclaus et al. 2005). The climatology
296 contains the annual cycle on a daily basis. Given an oceanic state at time t , the

297 anomalous sea surface condition \mathbf{y}' is derived by subtracting the actual oceanic state
 298 from the given climatological mean state. With this \mathbf{y}' and the anomalous flux forc-
 299 ing \mathbf{x}' at $t - 1$, EMAD produces the anomalous flux forcing at t . Adding this to
 300 the climatological mean forcing gives the net flux forcing at time t which is used to
 301 produce \mathbf{y}' at time $t + 1$.

302 It should be noted that since EMAD is only an approximation of ECHAM5, and
 303 since the $\mathcal{B}\mathbf{y}'$ -term is not a rigid restoring, the climatological mean state produced by
 304 the MPI-OM model coupled to EMAD generally does not match the climatological
 305 mean state produced by the fully coupled ECHAM5/MPI-OM. As a consequence, the
 306 time-mean of \mathbf{y}' is not zero. This non-zero time-mean of \mathbf{y}' can feed back to the fluxes
 307 and produce non-zero time-mean of \mathbf{x}' , whereby complicating the interpretation of
 308 the experiments to be introduced in Section 3. We will return to this issue later.

309 Apart from the feedbacks described by \mathcal{B} , there is no relaxation of salinity or
 310 temperature in the ocean. The only procedure used to prevent the ocean drifting
 311 away from the given climatological mean state is to restore the sea ice cover and
 312 sea ice thickness to that found in the integration with the ECHAM5/MPI-OM. The
 313 restoring time constant is chosen as 39 days.

314 **3 Numerical Experiments**

315 To study the effect of fluctuating daily fluxes, three experiments were carried out.
 316 In the experiment BH, MPI-OM was driven by the climatological mean fluxes of
 317 heat, fresh water and momentum plus an additional heat flux anomaly, H' , which

318 was obtained from $\mathcal{B}\mathbf{y}'$ with \mathbf{y}' representing SST anomalies. This particular form
 319 of $\mathcal{B}\mathbf{y}'$ contains the SST feedbacks that prevent large climate drifts. This is shown
 320 by an additional experiment in which the MPI-OM model was driven by the fixed
 321 climatological fluxes only. The ocean drifts to a warmer climate and produces a
 322 global mean surface temperature which is about 4 °C more (not shown) than that
 323 found in the coupled ECHAM5/MPI-OM run. The drift disappears when the $\mathcal{B}\mathbf{y}'$ -
 324 term is installed.

325 In the second experiment ABC, in which all the three terms in Eq.(1) are in-
 326 cluded, the MPI-OM model was forced with the same climatological mean fluxes plus
 327 fluctuating fluxes produced by EMAD. In the third experiment AB2C, MPI-OM was
 328 coupled to EMAD with the variance of white noise doubled.

329 The three experiments are summarized in Tab.1. For each experiment, a spin-up
 330 run of about 600 years was carried out. The spin-up runs started from the same
 331 initial state obtained from the coupled ECHAM5/MPI-OM model (Junglaus et
 332 al. 2005), after the ocean has reached a more or less statistically stationary state.
 333 Following the respective spin-up runs, the experiments were carried out for 200 years.
 334 The analysis given below is based on these 200-year integrations.

335 If all the three experiments produce the same climatological mean state (i.e. the
 336 same mean sea surface conditions and the same mean surface fluxes) and if this state
 337 is identical to that produced by the ECHAM5/MPI-OM model, the time-means of
 338 fluctuating fluxes in the three experiments will be zero. In this case, the difference
 339 between the experiments BH and ABC would describe the effect of fluctuating day-

340 to-day fluxes, and that between the experiments BH and AB2C would describe the
341 effect of enhanced fluctuating fluxes.

342 Unfortunately, the three experiments do not produce exactly the same climato-
343 logical mean state of the ECHAM5/MPI-OM model. Consequently, the time-mean
344 of fluctuating fluxes in experiments BH, ABC and AB2C are not zero. Moreover,
345 they differ from each other, since the climatological state in experiment BH can
346 differ from that obtained from experiment ABC or AB2C. Due to these differences,
347 the changes from experiment BH to ABC or from BH to AB2C are induced not only
348 by fluctuating fluxes included in experiment ABC and AB2C, but also by the dif-
349 ferences in the time-mean fluxes. A consideration of these time-mean fluxes reveals
350 some notable differences in the time-mean zonal wind stress (Figure 2). For instance,
351 there is an increase in zonal wind stress in the North Atlantic (at 30°W, 50°N) and
352 a northward shift of the mean zonal wind stress pattern over the Southern Ocean
353 from experiment BH to experiment ABC and AB2C. The increase in zonal wind
354 stress in the North Atlantic could be relevant, since the wind-driven gyre partici-
355 pates in the meridional salt transport and can therefore affect the MOC (Marti et
356 al. 2008). The shift in the Southern Ocean could contribute to the ACC differences
357 from experiment BH to ABC and to AB2C.

358 To assess the relevance of these non-zero time-mean fluxes, a supplementary
359 experiment, referred to as BH*, is carried out. Experiment BH* is identical to
360 experiment BH, except that the difference between the time-mean zonal wind stress
361 of experiment BH (Figure 2a) and that of experiment ABC (Figure 2b) is added to

the climatological mean wind forcing. It will be shown that the time-mean fluxes do not significantly affect the MOC changes and contribute only to a small part of ACC changes. Experiment BH* is integrated for 350 years.

4 Changes induced by fluctuating day-to-day fluxes

4.1 Time Evolutions

This subsection describes the time evolutions of the oceanic states in different experiments. The consideration is confined to the globally integrated sea surface temperature (SST) and two circulation indices, the Atlantic MOC-index and the ACC-index. The globally integrated SST is considered to describe the effect of the SST-feedback over time. The MOC-index and the ACC-index are chosen, since they characterize major global-scale circulations.

In all experiments, the SST time series are essentially statistically stationary (Figure 3a). The SST decreases slightly from experiment BH to experiment ABC and AB2C. The respective time-mean values are 18.57 °C, 18.15 °C and 18.12 °C. The spatial distribution of SST changes reveals decreases over most of the subtropical and mid-latitude oceans and increases partially over the North Atlantic from experiment BH to ABC and AB2C. The decrease is partly related to the increase in frequency and depth of convective events in the subtropical and mid-latitude oceans (see Section 4.4), which bring cold dense water down. The fluctuating fluxes also enhance the SST variability.

Figure 3b shows the time series of the MOC-index, defined as the maximum of the Atlantic meridional overturning streamfunction near 30°N at about 1220 m. The experiment BH (dotted line), which does not include fluctuating fluxes, reveals little variability in the MOC. Stronger variations are obtained by including fluctuations (solid line) in experiment ABC. The variations are strongest in experiment AB2C (dashed line) where the variance of the stochastic forcing is doubled.

Not only the variability but also the time mean of the MOC-index changes from experiment to experiment. This is further summarized in Tab.2. The smallest value of about 17 Sv is obtained from experiment BH. Inclusion of fluctuations leads to an increase of about 18 Sv in experiment ABC. Experiment AB2C, in which the strongest MOC of about 22 Sv is found, further confirms that the 1-Sv increase from experiment BH to experiment ABC is caused by the fluctuating component in the fluxes. The time-mean of the MOC-index of a 200-year time series of the coupled ECHAM5/MPI-OM simulation is also comparable to that of experiment ABC (last row in Tab.2).

Figure 3c shows the time series of the ACC-index defined as the mass transport through the Drake Passage. There is an enhancement of variability through fluctuations in experiment ABC and AB2C (solid line and dashed lines respectively). Concerning the time-mean (see also Tab.2.), a mean transport of about 200 Sv is obtained in experiment BH. This value is too high relative to the observed value of about 120 to 150 Sv (Nowlin and Klinck 1986 ; Cunningham et al. 2003). The transport reduces to about 148 Sv in experiment ABC and to about 122 Sv in AB2C.

404 The strength of the net mass transport through the Drake Passage reflects well the
405 strength of the zonal current in the entire Southern Ocean (not shown). Tab.2 shows
406 that a stronger MOC corresponds to a weaker ACC. The correspondence concerns
407 only the time-mean values. The variability of the ACC-index is not correlated to
408 that of the MOC-index.

409 To have an idea about how much of the changes listed in Tab.2 are caused by
410 the differences in the time-mean zonal wind stress shown in Figure 2, the time-
411 mean values of the MOC-index and the ACC-index are calculated from the last 200
412 years of experiment BH*. They amount to 17.2 Sv and 180 Sv, respectively. The
413 first number suggests that the increase in zonal wind stress in the North Atlantic
414 from Figure 2a to Figure 2b is not responsible for the 1-Sv MOC increase found by
415 comparing experiment ABC with experiment BH. Instead, the 1-Sv increase is likely
416 caused by the fluctuating fluxes included in experiment ABC. The second number
417 suggests that the ACC change from experiment BH to ABC is partly due to the
418 northward shift in the time-mean zonal wind stress shown in Figure 2b. However,
419 if the effect of time-mean wind stress and that of fluctuating fluxes can be linearly
420 superimposed, the effect due to the time-mean zonal wind stress is smaller than that
421 of the fluctuating fluxes.

422 For the comparison, the values of the MOC- and ACC-indices in ECHAM5/MPI-
423 OM are shown in Tab.2 (last row). If the climatological mean state in the ECHAM5/MPI-
424 OM model is identical to that in the hybrid EMAD/MPI-OM model, the values
425 obtained from experiment ABC would be close to those shown in the last row. One

426 finds a good agreement for the MOC-index, but not as good an agreement for the
427 ACC-index. This further confirms that the circulation in the MPI-OM model is
428 more sensitive to the time-mean zonal wind stresses in the Southern Ocean than
429 those in the North Atlantic.

430 4.2 Changes in the Atlantic Meridional Overturning Circulation

431 The different formulations of the surface fluxes result in different Atlantic meridional
432 overturning circulations (Figure 4). The difference concerns not only the strength
433 that is described by the MOC-index in Figure 3 and Tab.2., but also the structure.
434 When the MPI-OM is driven by the climatological fluxes plus the oceanic feed-
435 backs (experiment BH), an overturning cell of around 2800 m and 17 Sv maximum
436 strength is obtained (Figure 4a). In experiment ABC (Figure 4b), the overturning
437 cell is stronger and extends a couple of hundreds of meters down to the deep ocean
438 compared to that of BH. When the stochastic forcing is doubled, the overturning
439 circulation further strengthens and deepens (Figure 4c). The deepening of the over-
440 turning cell is accompanied by the weakening of the Antarctic Bottom Water cell
441 and the retreat of the Antarctic Bottom Water (AABW). In experiment AB2C,
442 the penetration of AABW into the abyssal North Atlantic is severely blocked. The
443 spatial structure of the Atlantic MOC in experiment ABC is comparable to that
444 produced by the ECHAM5/MPI-OM model (not shown) and that obtained from an
445 ensemble of coupled AOGCMs (Stouffer et al. 2006).

446 To make sure that the 1-Sv increase in MOC is statistically significant, a t-test

447 is carried out. The null hypothesis that the maximum overturning in experiment
448 BH equals that in experiment ABC is considered. The null hypothesis is rejected
449 with 1% risk.

450 To show that the above described structural changes do not result from the
451 different time-mean zonal wind stress, the mean Atlantic overturning streamfunction
452 obtained from the last 200 years of experiment BH* is shown in Figure 5. Both the
453 strength and the structure are comparable to the streamfunction obtained from
454 experiment BH.

455 4.3 Changes in the density fields

456 To understand whether and to what extent fluctuating fluxes change the mean cir-
457 culation via changing density structures, consider first the situation at the surface.
458 Figure 6a shows the zonal-mean meridional profiles of surface density in the Atlantic
459 sector. The large differences at the high northern latitudes result from different
460 climatological mean states in the Arctic: the Arctic becomes more saline from ex-
461 periment BH to experiment ABC and AB2C (not shown). In the North Atlantic
462 from about 40°N to 75°N, it is difficult to relate changes in the meridional density
463 gradient to the MOC changes found in experiments BH, ABC and AB2C. In the
464 south from 30°S to 60°S, the meridional gradient in experiment BH is stronger than
465 that in experiment ABC and AB2C, as indicated by the dotted line (BH) which
466 is below the solid (ABC) and dashed (AB2C) lines north of about 45°S and above
467 them, south of 45°S. The change from experiment ABC to AB2C (solid and dashed

lines) is less clear. Following the previous studies (e.g. Russell et al. 2006) suggesting that the ACC is related to the density gradient in deeper layers, in particular to the density gradient integrated over the sill depth, density changes in the oceanic interior were considered.

Indeed the effects of fluctuating fluxes can be traced down to the deep ocean. Figure 7a shows the in-situ density in experiment BH at 1365 m. The density field is characterized by higher density in the Atlantic and the Southern Oceans than in the Pacific and the Indian Oceans. To describe the changes in the density gradient induced by fluctuating fluxes, the differences between experiments ABC and BH and between AB2C and BH are shown in Figure 7b and c, respectively. The dominant feature of the density changes is the zonally oriented density increases centered near 40°S and density decreases further south. The amplitudes of the density increases are larger than those of decreases. These changes lead to a reduction in the meridional density gradient in the Southern Ocean and hence a weakening of the ACC.

The density changes in the North Atlantic are more subtle. From the difference AB2C-BH shown in Figure 7c, one can identify a few isolines in the Atlantic north of 40°N that reveal strong tilt in the north-south direction. These isolines suggest an increase in the zonal density gradient that are by geostrophic relation consistent with the large increase of the MOC of more than 4 Sv from experiment BH to AB2C. However, this feature does not show up clearly in the difference ABC-BH (Figure 7b).

A further search for a clear relation between changes in density distribution and

490 changes in the Atlantic MOC leads to the consideration of the depth-integrated in-
 491 situ density. This quantity was shown to be related to the strength of the MOC
 492 in previous studies (Hughes and Weaver, 1994 and Thorpe et al 2001). Figure 6b
 493 shows the zonal mean of depth-integrated in-situ density in the Atlantic sector. The
 494 increase of the density equatorward of about 40° from experiment BH to ABC and
 495 AB2C is related to the change in the climatological mean state, which becomes colder
 496 in experiment ABC and AB2C, relative to that in experiment BH. The cooling is
 497 partly due to the increase in frequency and depth of convective events (see Section
 498 4.4). Regarding the meridional gradient, the meridional gradients between 40°S and
 499 40°N and between 40°N and 60°N do not change much. However, small changes
 500 in density difference between northern North Atlantic and the South Atlantic are
 501 possible. After calculating the density difference between different latitudinal strips
 502 in the North and South Atlantic, we found that the density difference between the
 503 northern strip extending from 55°N to 60°N and the southern strip extending from
 504 45°S to 50°S increases with the MOC from 0.11 kg/m^3 in experiment BH to 0.12
 505 kg/m^3 in experiment ABC and to 0.13 kg/m^3 in experiment AB2C. A similar north-
 506 south density difference was considered in studies by Rahmstorf (1996) and Thorpe
 507 et al (2001).

508 In the Southern Ocean, the meridional gradient of the depth-integrated density
 509 (Figure 6b) is reduced. Expressed in terms of the density difference between 40°S
 510 and 60°S , one finds decreases from 1.02 kg/m^3 in experiment BH (dotted) to 0.77
 511 kg/m^3 in experiment ABC (solid) and to 0.63 kg/m^3 in experiment AB2C (dashed).

512 The reduction of meridional gradient is more strongly related to the increase in
 513 density around 40°S than to the decrease in density around 60°S. These changes
 514 in meridional density distribution are related to the changes in ACC in different
 515 experiments by the geostrophic relation.

516 4.4 Changes in the vertical mixing

517 In this section, the way surface fluxes alter the density in the deep ocean is examined.
 518 It will be shown that surface fluxes change the density via vertical mixing. Before
 519 dealing with these mixing changes, consider first the time-mean mixing, as described
 520 by the time-mean vertical diffusion coefficient K for experiment BH at 285 m depth
 521 in Figure 8a and at 900 m depth in Figure 9a. In GIN Seas and along and near
 522 the Antarctic coast in the Atlantic sector and south of the South America, large
 523 time-mean values of K and mean convection depth (Figure 10a) are found, which is
 524 also the case in the coupled ECHAM5/MPI-OM model. These regions are the most
 525 unstable regions of the ocean model. Elsewhere, the modelled ocean is much more
 526 stable.

527 A maximum of K is also found at 285 m in the north Pacific just west of the
 528 date line between 50°N and 60°N (Figure 8a). This maximum disappears at 900 m
 529 in Figure 9a. The map of the mean depth of convection (Figure 10a) suggests that
 530 the convection related to this maximum is shallower than 600-650 m.

531 Generally, K is smaller than $0.002 \text{ m}^2/\text{s}$ in most part of the ocean at 900 m and
 532 decreases with depth to values smaller than $10^{-4} \text{ m}^2\text{s}^{-1}$ below 2500 m. These values

533 should be compared with the observational range of 10^{-6} to $10^{-3} \text{ m}^2/\text{s}$ reported from
534 interior oceanic regions (Ledwell et al. 1993; Moum et al. 2002, Gregg et al. 2003,
535 Ledwell et al. 2000, Sloyan 2005).

536 Consider now the changes in the vertical mixing due to different surface fluxes.
537 In the following, the effect of the fluctuating fluxes is indicated by the difference in K
538 (ABC-BH) obtained from experiment ABC and BH. The effect of the fluctuations
539 with enhanced variance is obtained by comparing the difference AB2C-BH with
540 the difference ABC-BH. The possible effect of the time-mean zonal wind stress on
541 changes in K is small and will be discussed at the end of this section.

542 Figure 8b shows the difference in K (ABC-BH) at 285 m depth, induced by the
543 fluctuations. Outside the tropics, where large changes of K are found, there is a
544 striking correspondence between the distribution of the time-mean frequency and
545 depth of convective events shown in Figure 8a and Figure 10a and the distribution
546 of the changes in K from experiment BH to ABC shown in Figure 8b in the MPI-
547 OM model: The strong decreases in K are found in the regions where the time-
548 mean values of K are large, indicating frequent occurrence of convective events due
549 to mostly unstable stratification. These regions consist of the GIN Seas, an area
550 centered near 50°W and 35°N in the North Atlantic, the areas south of the South
551 American continent and west and east of the Antarctic Peninsula. The increases
552 in K , on the other hand, are found in regions where the time-mean values of K
553 are generally small and convective events are less frequent due to mostly stable
554 stratification. In the North Atlantic, an area with increases in K is found between

555 40°N to 60°N, south of the GIN Seas. There, the time-mean values of K are generally
556 small, apart from the areas close to the Irminger Sea which will be discussed at the
557 end of this section. In the Southern Ocean, increases in K are found mainly in the
558 latitude band from 20°S to 50°S. This correspondence between the time-mean values
559 of K and changes in K can also be seen in experiment AB2C (Figure 8c).

560 At 900 m (Figure 9b), the correspondence between the time-mean mixing and
561 the changes in the convective mixing is also noticeable poleward of about 40°. In
562 particular, the decreases in K are mainly located in regions with large values of the
563 time-mean mixing shown in Figure 9a. Overall, the magnitudes of mixing changes
564 are much smaller at 900 m (Figure 9b,c) than at 285 m (Figure 8b,c). The areas
565 with enhanced mixing in experiment ABC (Figure 9b) is enlarged when the strength
566 of stochastic fluctuations is doubled in experiment AB2C (Figure 9c): The patchy
567 structure over the Southern Ocean in Figure 9b becomes more uniform in Figure
568 9c. Mixing structures similar to Figure 9 but with smaller amplitudes can be found
569 down to about 2500 to 3000 m. Further below, the mixing signal is much less zonally
570 oriented.

571 Following the definition of K , the above described changes in K are related
572 to changes in the *frequency* of convective events. Changes in the mean *depth* of
573 convective events are described in Figure 10b and c. The largest changes in the
574 mean convection depth are about 300 m. A comparison of Figure 10b,c with Figure
575 8b,c suggests that, apart from the tropical oceans, an increase (a decrease) in the
576 frequency of convective events corresponds to an increase (a decrease) in the depth

577 of convective events. Since the regions with small (large) time-mean values of K and
578 shallow (deep) mean convection represent regions which are often stably (unstably)
579 stratified, one can conclude that the fluctuating fluxes tend to increase the convective
580 mixing over mostly stable ocean and decrease convective mixing over mostly unstable
581 ocean. Moreover, an increase (a decrease) in convective mixing is accomplished by
582 an increase (a decrease) in both frequency and depth of convective events.

583 The above described mixing changes can be responsible for the density changes
584 described in Section 4.3. As the enhanced vertical mixing is related to an increase
585 in the frequency and the depth of convective events and these events generally bring
586 dense water down, the increase in vertical mixing in the midlatitudes found in ex-
587 periments ABC and AB2C can lead to an increase in density there. In the Atlantic,
588 the increase in the vertical mixing near the northern strip 55°N - 60°N is stronger
589 than that in the southern strip 45°S - 50°S . This can lead to the increase of the den-
590 sity difference between the two strips from experiment BH to experiment ABC and
591 AB2C, which is related to the respective MOC increases. The large-scale increase
592 in the vertical mixing in the Southern Ocean can be responsible for the increase
593 in density near 40°S , which results in a weaker meridional density gradient and a
594 weaker ACC.

595 There exists a few spots where the change in K is not clearly related to the mean
596 stratification, for instance west of Svalbard and also in the Arctic.

597 Note that the distribution of changes in the convection depth (Figure 10b, c)
598 compares less well with changes in K at 900 m (Figure 9b, c) than with changes

599 at 285 m (Figure 8b, c). This is because Figure 10 represents the mean convection
600 depth, rather than the depth of individual convective events. Apart from a few
601 exceptions at high-latitudes, convective events are mostly shallower than a few hun-
602 dred meters. The changes in convection depth due to fluctuating fluxes are generally
603 smaller than 300 m. Thus, Figure 10b and c reflect mainly the changes related to
604 convections shallower than 900 m.

605 Also in tropical oceans, the changes in convective activity (Figure 10b,c) do
606 not correspond to changes in K (Figure 8b,c and Figure 9b,c) in tropical oceans.
607 There, one finds increases in the convective depth, even though the vertical mixing
608 is reduced. This is because convective events are confined to the upper 60 m in the
609 tropical and subtropical Atlantic and Indian Oceans and to the upper 100 m in the
610 tropical and subtropical Pacific, but can reach a few hundred meters in the extra-
611 tropical regions. As the convective events triggered by the fluctuating daily fluxes
612 are confined to a shallow surface layer, the decrease in K in the tropics below, say,
613 100 m, as seen in Figure 8b,c and Figure 9b,c is likely caused by the Ri -dependent
614 mixing, rather than the convective mixing.

615 The above described mixing changes are mainly due to fluctuating fluxes. The
616 effect of time-mean fluxes is mostly secondary. This is shown by the difference in
617 the mean convection depth found in the experiments ABC and BH* (Figure 11).
618 Different from Figure 10b which shows changes due to fluctuating fluxes *and* the
619 difference in the time-mean zonal wind stress, the effect due to different time-mean
620 zonal wind stress is eliminated in Figure 11. Since Figure 10b is very close to

Figure 11, the effect due to different time-mean zonal wind stress must be small. An exception is the change near the Irminger Sea. In this region, the mechanism which alters the MOC through the wind-driven gyre (Marti et al. 2008) can be at work. The stronger time-mean zonal wind stress in experiment ABC can transport more salt northward, whereby enhancing the surface density and triggering more often convective events. This is likely the reason, why large increases in the frequency and depth of convective events are found in the Irminger Sea (Figure 8b and Figure 10b), where, if the effect of fluctuating fluxes dominated, a decrease in the frequency and depth of convective events was expected.

5 Conclusions and discussion

The MPI-OM model coupled to the empirical flux model EMAD is used to isolate the effect of fluctuating fluxes. It is found that fluctuating daily fluxes can produce a 1-Sv-increase in the strength of the Atlantic MOC, which is about 7% of the MOC obtained without the fluctuating fluxes, and a 32-Sv-reduction of the ACC, which is about 16% of the ACC obtained without fluctuating fluxes. These changes exclude (with the aid of experiment BH*) the effect of non-zero time-mean fluxes that cannot be completely excluded from the experiments. The MOC changes are related to the change in the meridional density difference between two latitudinal strips in the northern North Atlantic and in the South Atlantic, defined in a way similar to that in Rahmstorf (1996) and Thorpe et al (2001). The ACC changes are related to a reduction in meridional gradient in the depth-integrated density.

642 These density changes are likely caused by changes in vertical mixing induced
643 by fluctuating surface fluxes. In the MPI-OM model, large changes in the vertical
644 mixing are related to the changes in the convective mixing. Fluctuating fluxes alter
645 convective mixing in a non-linear way. In the mostly unstable regions, e.g. in
646 the GIN Seas and near the Antarctic Peninsula, positive buoyancy anomalies can
647 restrain convective events, whereas negative buoyancy anomalies do not significantly
648 affect the convective behaviour, leading to an overall reduction in the convective
649 mixing. In mostly stable regions, e.g. in the subtropical and mid-latitude oceans,
650 large negative buoyancy anomalies can trigger additional convective events, whereas
651 positive buoyancy anomalies do not significantly change the convective behaviour,
652 leading to an overall strengthening of the convective mixing.

653 The conclusions about the effect of fluctuating fluxes on the convective mixing
654 are drawn within the framework of a coarse resolution version of the MPI-OM. In
655 another OGCM, which produces a different stratification with a different distribution
656 of convective activity, the effect of fluctuating fluxes on the convective mixing, which
657 is closely related to the mean stratification, can be different. As a consequence, the
658 exact numbers concerning the changes in the MOC and ACC due to the fluctuating
659 fluxes can depend on the model used. Nevertheless, the mechanism through which
660 fluctuating daily fluxes alter the convective mixing should operate in other models,
661 and probably also in nature.

662 ACKNOWLEDGMENTS

663 This study is supported by the German Research Foundation in the Special
664 Research Areas (SFB 512), “Cyclones and the North Atlantic Climate System”. We
665 thank Uwe Mikolajewicz and two anonymous reviewers for valuable suggestions in
666 improving this manuscript. Thanks also to Johann Jungclaus who provided us a
667 program to calculate the volume transports between the Nordic Seas and the North
668 Atlantic which helped us to answer a question raised by a reviewer.

669 REFERENCES

- 670 Cunningham S, Alderson S, King BA, Brandon MA (2003) Transport and variabil-
671 ity of the ACC. *J Geophys Res* 108. doi:10.1029/2001JC001147
- 672 Frankignoul C, Czaja A, L’Heveder B (1998) Air-sea feedback in the North Atlantic
673 and surface boundary conditions for ocean models. *J Clim* 11:2310-2324
- 674 Gent PR, Willebrand J, McDougall J, McWilliams JC (1995) Parameterising eddy
675 induced tracer transports in ocean circulation models. *J Phys Oceanogr* 25:463-
676 474
- 677 Gregg M, Sanford T, Winkel D (2003) Reduced mixing from the breaking of internal
678 waves in equatorial waters. *Nature* 422:513-515
- 679 Griffies SM (1998) The Gent-McWilliams skew flux. *J Phys Oceanogr* 28:831-841
- 680 Haak H, Jungclaus JH, Mikolajewicz U, Latif M (2003) Formation and propagation
681 of great salinity anomalies. *Geophys Res Lett* 30. doi:10.1029/2003GL017065
- 682 Hughes T, Weaver A (1994) Multiple equilibrium of an asymmetric two-basin
683 model. *J Phys Oceanogr* 24:619-637
- 684 Jungclaus JH, Haak H, Latif M, Mikolajewicz U (2005) Arctic-North Atlantic inter-
685 actions and multidecadal variability of the meridional overturning circulation.
686 *J Clim* 18:4013-4031
- 687 Kuhlbrodt T, Griesel A, Montoya M, Levermann A, Hoffmann M, Rahmstorf, S

688 (2007) On the driving processes of the oceanic meridional overturning circula-
 689 tion. *Rev Geophys* 45. doi:10.1029/2004RG000166

690 Kuhlbrodt T, Monahan A (2003) Stochastic stability of open-ocean deep convec-
 691 tion. *J Phys Oceanogr* 33:2764-2780

692 Ledwell J, Montgomery E, Polzin K, St.Laurent, Schmitt L, Toole J (2000) Evi-
 693 dence for enhanced mixing over rough topography in the abyssal ocean. *Nature*
 694 403:179-182

695 Ledwell J, Watson A, Law C (1993) Evidence for slow mixing across the pycnocline
 696 from an open-ocean tracer release experiment. *Nature* 364:701-703

697 Legutke S, Voss R (1999) The Hamburg atmosphere-ocean coupled circulation
 698 model ECHO-G. DKRZ, Tech. Rep. 18, Hamburg, Germany

699 Marsland SJ, Haak H, Jungclaus JH, Latif M, Roeske F (2003) The Max-Planck-
 700 Institute global ocean/sea ice model with orthogonal curvilinear coordinates.
 701 *Ocean Model* 5:91-127

702 Marti O, Braconnot P, Dufresne J-L, Bellier J, Benshila R, Bony S, Brockmann P,
 703 Cadule P, Caubel A, Codron F, de Noblet N, Denvil S, Fairhead L, Fichefet T,
 704 Foujols M-A, Friedlingstein P, Goosse H, Grandpeix J-Y, Guilyardi E, Hourdin
 705 F, Krinner G, Lvy C, Madec G, Mignot J, Musat I, Swingedouw D, Talandier
 706 C (2009) Key features of the IPSL ocean atmosphere model and its sensitivity
 707 to atmospheric resolution. *Clim Dyn* (submitted)

708 Moum J, Caldwell D, Nash J , Gunderson G (2002) Observations of boundary
709 mixing over the continental slope. *J Phys Oceanogr* 32:2113-2130

710 Munk W, Wunsch C (1998) Abyssal recipes II. Energetics of tidal and wind mixing.
711 *Deep Sea Res I* 45:1977-2010

712 Nowlin WDJ, Klinck JM (1986) The physics of the ACC. *Rev Geophys* 24:469-491

713 Pacanowski RC, Philander SGH (1981) Parameterisation of vertical mixing in nu-
714 merical models of tropical oceans. *J Phys Oceanogr* 11:1443-1451

715 Rahmstorf S (1995) Multiple convection patterns and thermohaline flow in an ide-
716 alized OGCM. *J Clim* 8:3028-3039

717 Rahmstorf S, Willebrand J (1995) The role of temperature feedback in stabilizing
718 the thermohaline circulation. *J Phys Oceanogr* 25:787-805

719 Rahmstorf S (1996) On the freshwater forcing and transport of the Atlantic ther-
720 mohaline circulation. *Clim Dyn* 12:799-811

721 Raible C, Luksch U, Fraedrich K, Voss R (2001) North Atlantic decadal regimes in
722 a coupled GCM simulation. *Clim Dyn* 18:321-330

723 Redi MH (1982) Oceanic isopycnal mixing by coordinate rotation. *J Phys Oceanogr*
724 12:1154-1158

725 Russell JL, Stouffer RJ, Dixon KW (2006) Intercomparison of the southern ocean
726 circulations in IPCC coupled model control simulations. *J Clim* 19:4560-4575

727 Sloyan BM (2005) Spatial variability of mixing in the Southern Ocean. *Geophys*
728 *Res Lett* 32. doi:10.1029/2005GL023568

729 Stouffer RJ, Yin J, Gregory JM, Dixon KW, Spelman MJ, Hurlin W, Weaver AJ,
730 Eby M, Flato GM, Hasumi H, Hu A, Jungclaus JH, Kamenkovich IV, Lever-
731 mann A, Montoya M, Murakami S, Nawrath S, Oka A, Peltier WR, Robitaille
732 DY, Sokolov A, Vettoretti G, Webber SL (2006) Investigating the causes of the
733 response of the thermohaline circulation to past and future climate changes.
734 *J Clim* 19:1365-1387

735 Swingedouw D, Braconnot P, Delecluse P, Guilyardi E, Marti O (2007) Quantifying
736 the AMOC feedbacks during a 2xCO₂ stabilization experiment with land - ice
737 melting. *Clim Dyn* 29:521-534

738 Thorpe RB, Gregory JM, Johns TC, Wood RA, Mitchell JFB (2001) Mechanisms
739 determining the Atlantic thermohaline circulation response to greenhouse gas
740 forcing in a non-flux adjusted coupled climate model. *J Clim* 14:3102-3116

741 Toggweiler JR, Samuels B (1995) Effect of Drake Passage on the global thermoha-
742 line circulation. *Deep Sea Res* 42:477-500

743 Tziperman E (1986) On the role of interior mixing and air sea fluxes in determining
744 the stratification and circulation of the oceans. *J Phys Oceanogr* 16:680-693

745 von Storch J-S (2000) Signatures of air-sea interactions in a coupled atmosphere-
746 ocean GCM. *J Clim* 13:3361-3379

- 747 von Storch J-S, Montavez JP, Beena BS (2005) EMAD: An empirical model of
748 air-sea fluxes. Meteor Zeitschrift 14:755-762
- 749 Walin G (1982) On the relation between sea-surface heat flow and thermal circu-
750 lation in the oceans. Tellus 34:187-195
- 751 Webb DJ, Suginohara N (2001) Vertical mixing in the ocean. Nature 409:37

752 FIGURE CAPTIONS

753 Figure 1: Daily snapshots of wind stress and heat flux anomalies from a) EMAD
754 model and b) NCEP/NCAR Reanalysis. The units are in *Pascal* and W/m^2
755 respectively.

756 Figure 2: Time-mean zonal wind stress in *Pa* obtained in a) experiment BH, b)
757 experiment ABC and c) experiment AB2C.

758 Figure 3: Yearly time series of a) globally integrated sea surface temperature in $^{\circ}C$,
759 b) the maximum of Atlantic meridional overturning streamfunction located
760 near $30^{\circ}N$ in *Sv* (MOC-index) and c) Drake Passage mass transport in *Sv*
761 (ACC-index) obtained from experiment BH (dotted), ABC (solid) and AB2C
762 (dashed).

763 Figure 4: Spatial structure of the time-mean Atlantic MOC in *Sv* in different
764 experiments.

765 Figure 5: Spatial structure of the time-mean Atlantic MOC in *Sv* in experiment
766 BH*.

767 Figure 6: Meridional profiles of the zonal mean of surface density and the zonal
768 mean of depth-integrated in-situ density in the Atlantic sector obtained from
769 experiment BH (dotted), ABC (solid) and AB2C (dashed). The depth inte-
770 gration starts from 1220 m for experiments BH, ABC and AB2C. The Atlantic
771 sector covers the oceanic region from $70^{\circ}W$ to $10^{\circ}E$ and hence includes the
772 Drake passage. Unit is kg/m^3 .

773 Figure 7: Horizontal distributions of in situ density at 1365 m in kg/m^3 for a) the
774 time-mean in experiment BH and b) the difference between experiments ABC
775 and BH and c) between experiments AB2C and BH.

776 Figure 8: Horizontal distributions of K at 285 m in m^2/s for a) the time-mean in
777 experiment BH and b) the difference between experiments ABC and BH and
778 c) between experiments AB2C and BH.

779 Figure 9: Same as Figure 8, but for K at 900 m.

780 Figure 10: Horizontal distributions of mean convection depth in m for a) the time-
781 mean in experiment BH and b) the difference between experiments ABC and
782 BH and c) between experiments AB2C and BH.

783 Figure 11: Horizontal distribution of the change in the mean convection depth in
784 m between experiments ABC and BH*.

785 TABLE CAPTIONS

786 Table 1 : Experiments done with MPI-OM driven by different types of daily fluxes
787 at the sea surface. $\bar{\mathbf{x}}$ denotes the climatological fluxes and \mathbf{x}' the flux anomalies
788 predicted by different versions of EMAD model.

789 Table 2 : 200-year means of MOC-index and ACC-index in Sv in different experi-
790 ments.

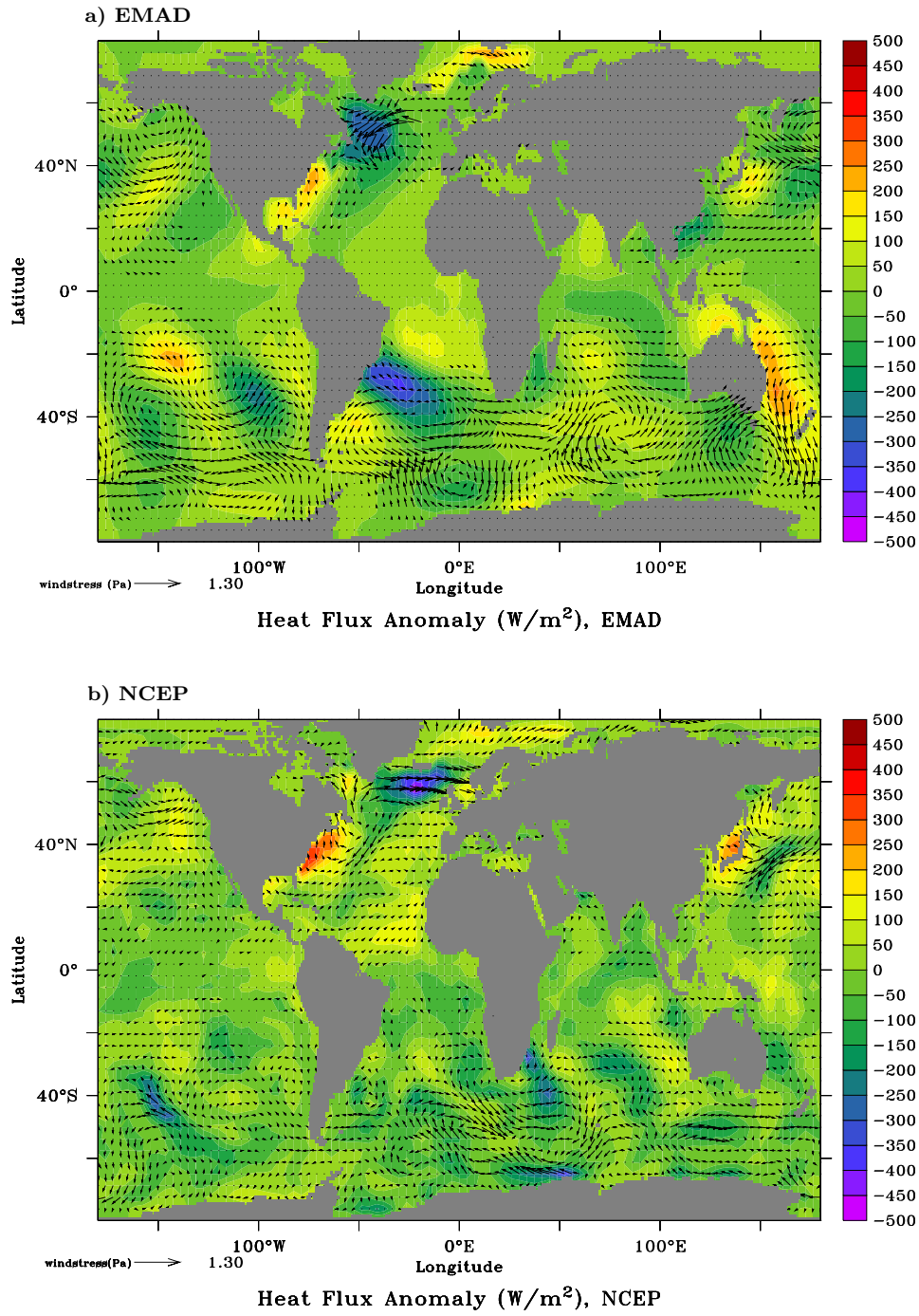


Figure 1: Daily snapshots of windstress and heatflux anomalies from a) EMAD model and b) NCEP/NCAR Reanalysis. The units are in *Pascal* and W/m^2 respectively.

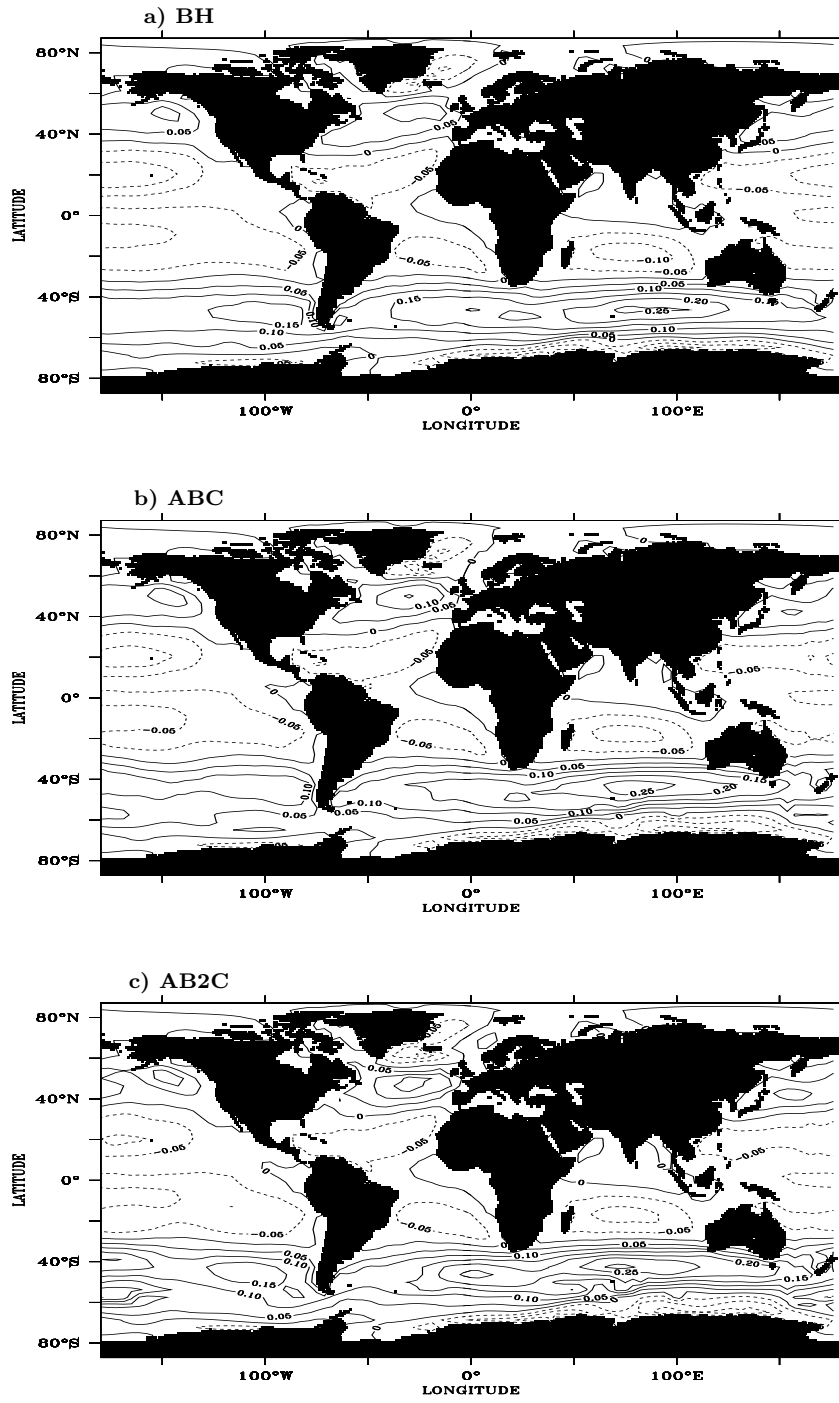


Figure 2: Time-mean zonal wind stress in Pa obtained in a) experiment BH, b) experiment ABC and c) experiment AB2C.

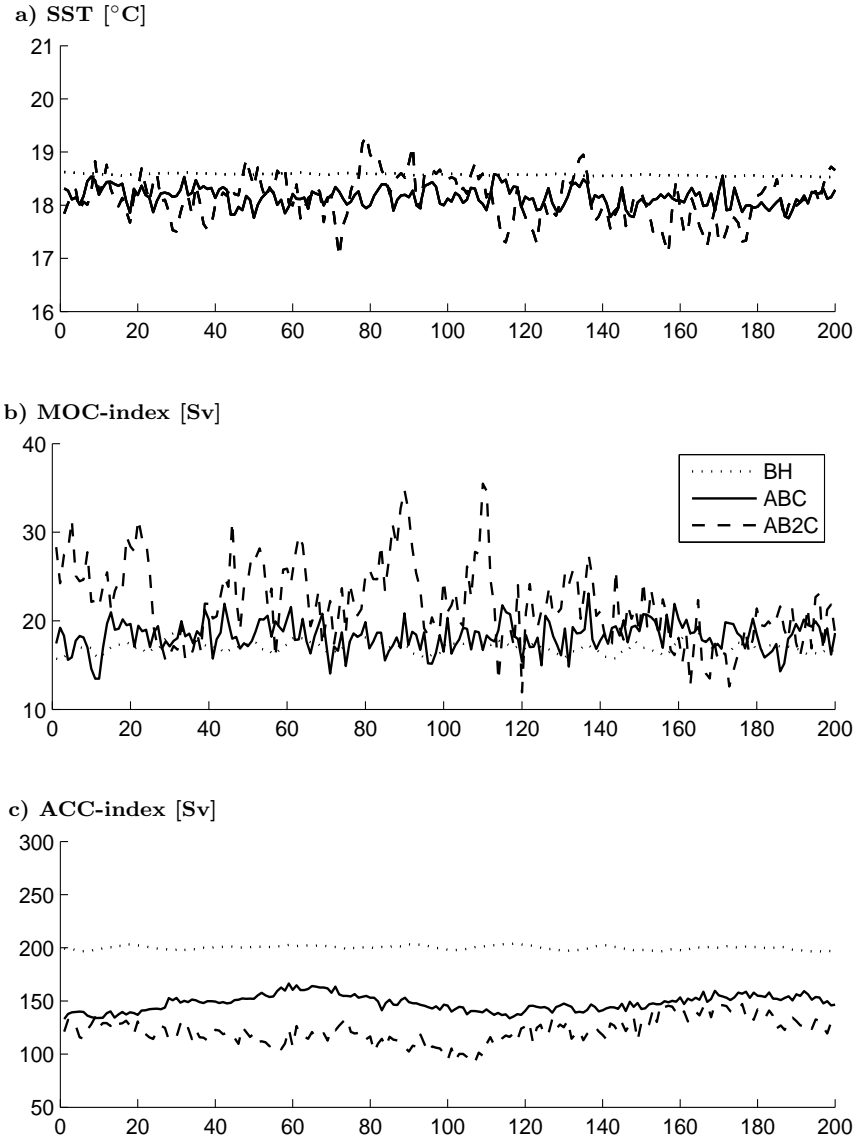


Figure 3: Yearly time series of a) globally integrated sea surface temperature in $^{\circ}\text{C}$, b) the maximum of Atlantic meridional overturning streamfunction located near 30°N in Sv (MOC-index) and c) Drake Passage mass transport in Sv (ACC-index) obtained from experiment BH (dotted), ABC (solid) and AB2C (dashed).

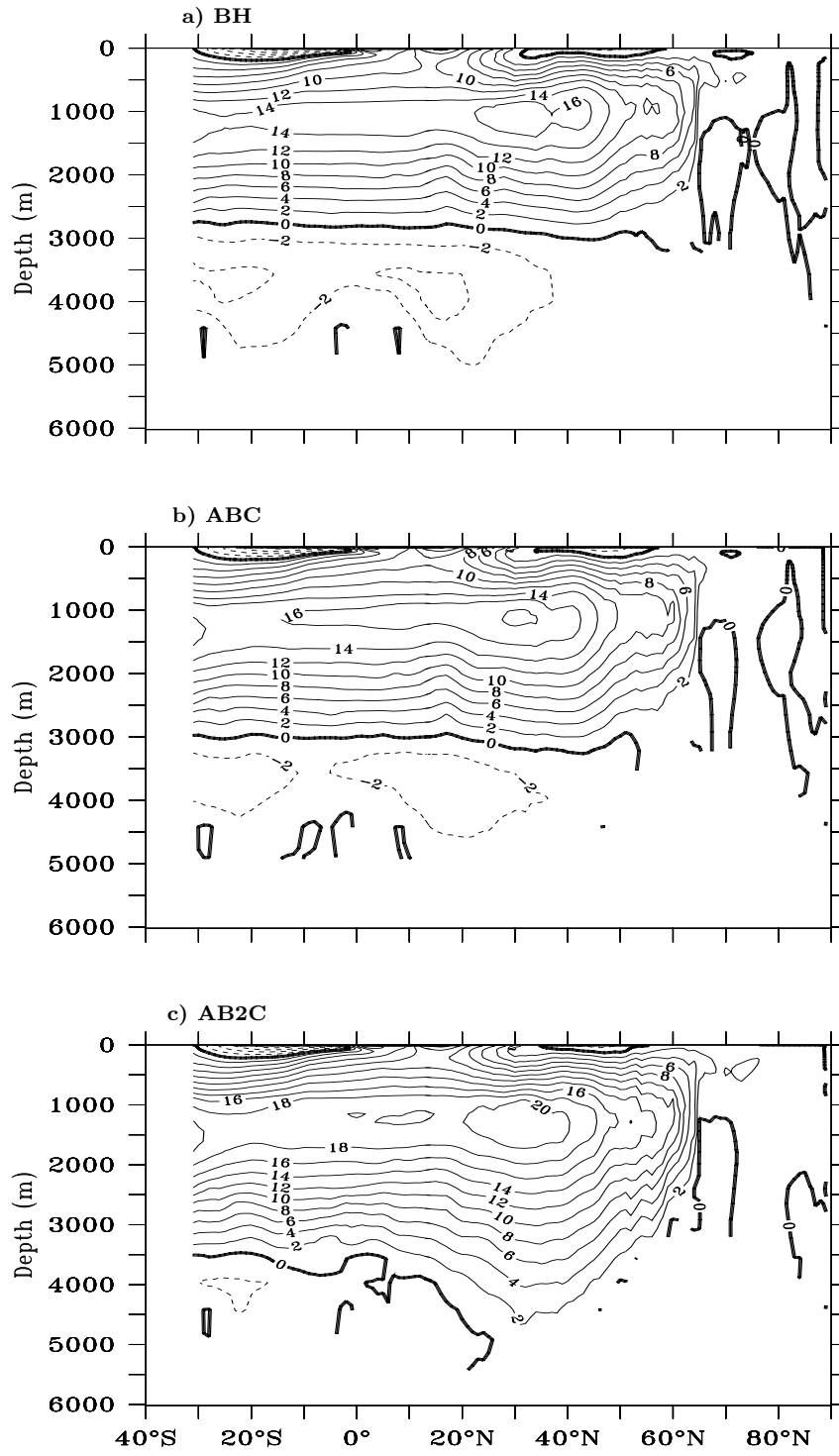


Figure 4: Spatial structure of the time-mean Atlantic MOC in Sv in different experiments.

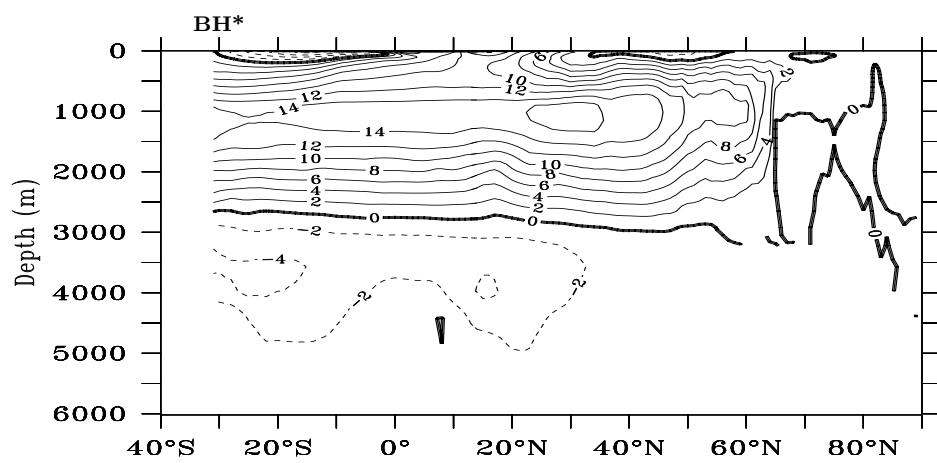


Figure 5: Spatial structure of the time-mean Atlantic MOC in Sv in experiment BH*.

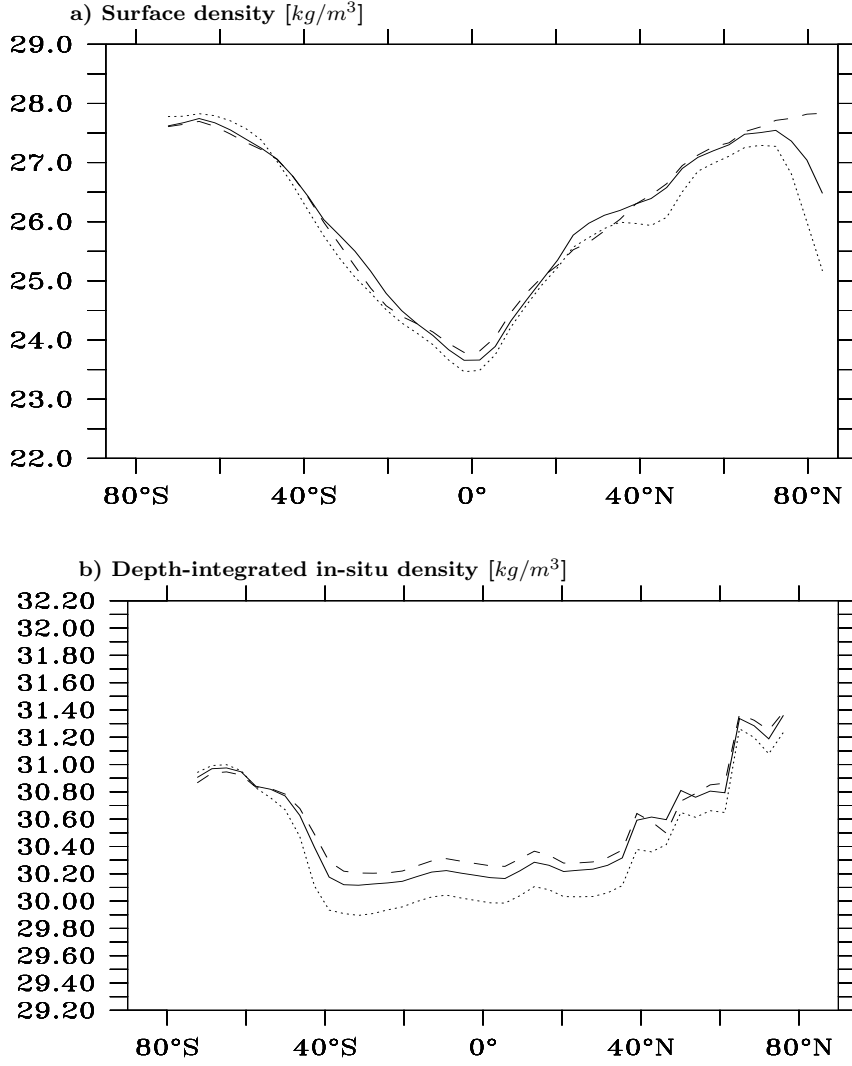


Figure 6: Meridional profiles of the zonal mean of surface density and the zonal mean of depth-integrated in-situ density in the Atlantic sector obtained from experiment BH (dotted), ABC (solid) and AB2C (dashed). The depth integration starts from 1220 m for experiments BH, ABC and AB2C. The Atlantic sector covers the oceanic region from 70°W to 10°E and hence includes the Drake passage. Unit is kg/m^3 .

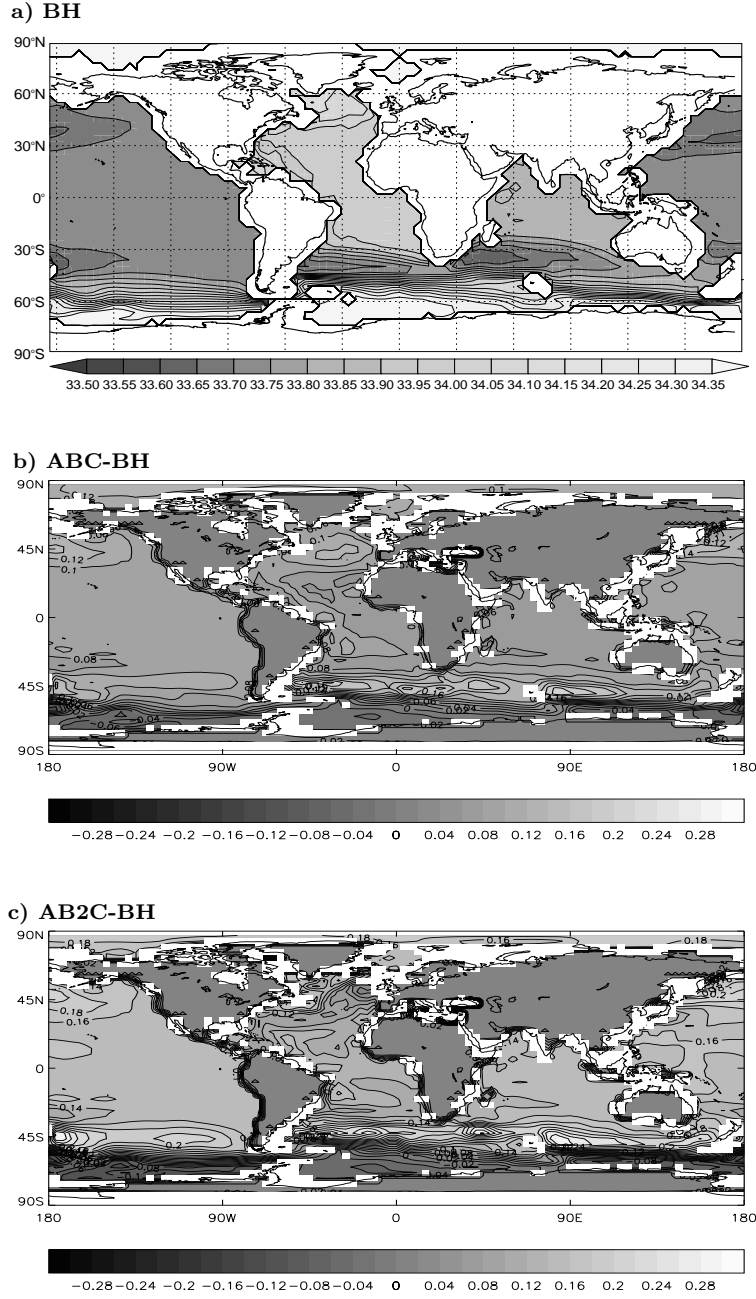


Figure 7: Horizontal distributions of a) the time-mean in situ density at 1365 m in experiment BH and b) the difference between density in experiments ABC and BH and c) between experiments AB2C and BH. The unit is kg/m^3 .

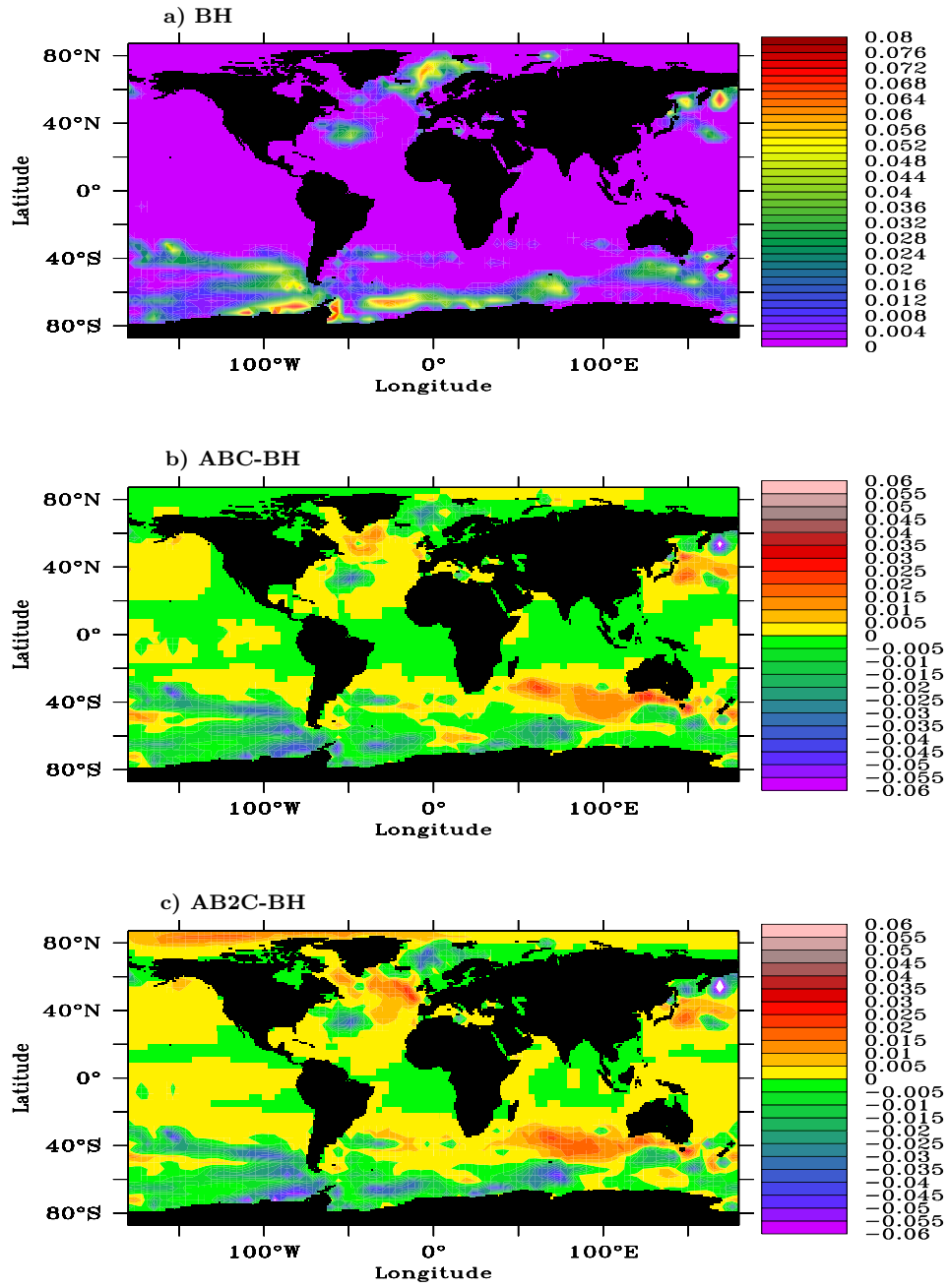


Figure 8: Horizontal distributions of K at 285 m in m^2/s for a) the time-mean in experiment BH and b) the difference between experiments ABC and BH and c) between experiments AB2C and BH.

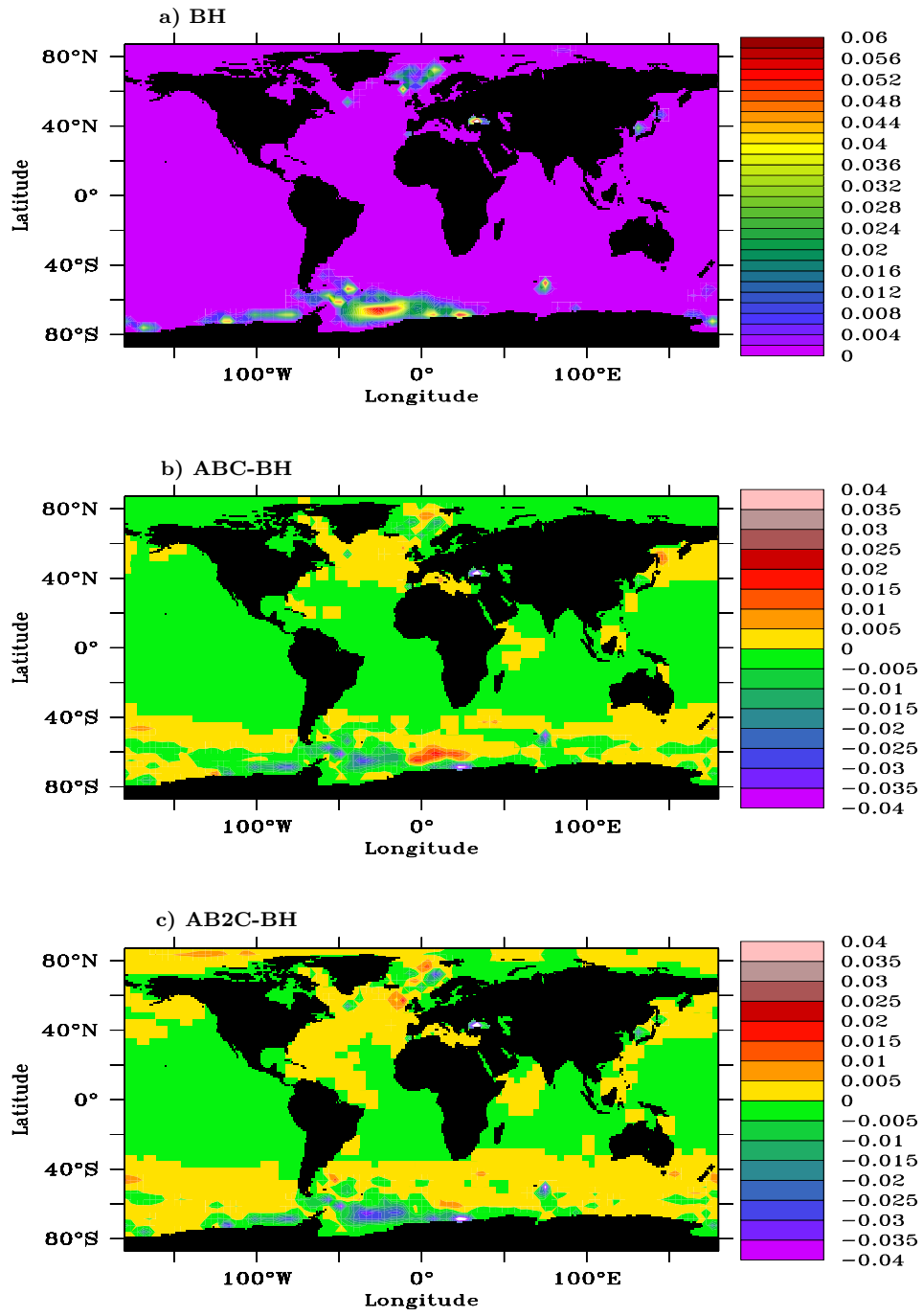


Figure 9: Same as Figure 8 but for K at 900 m.

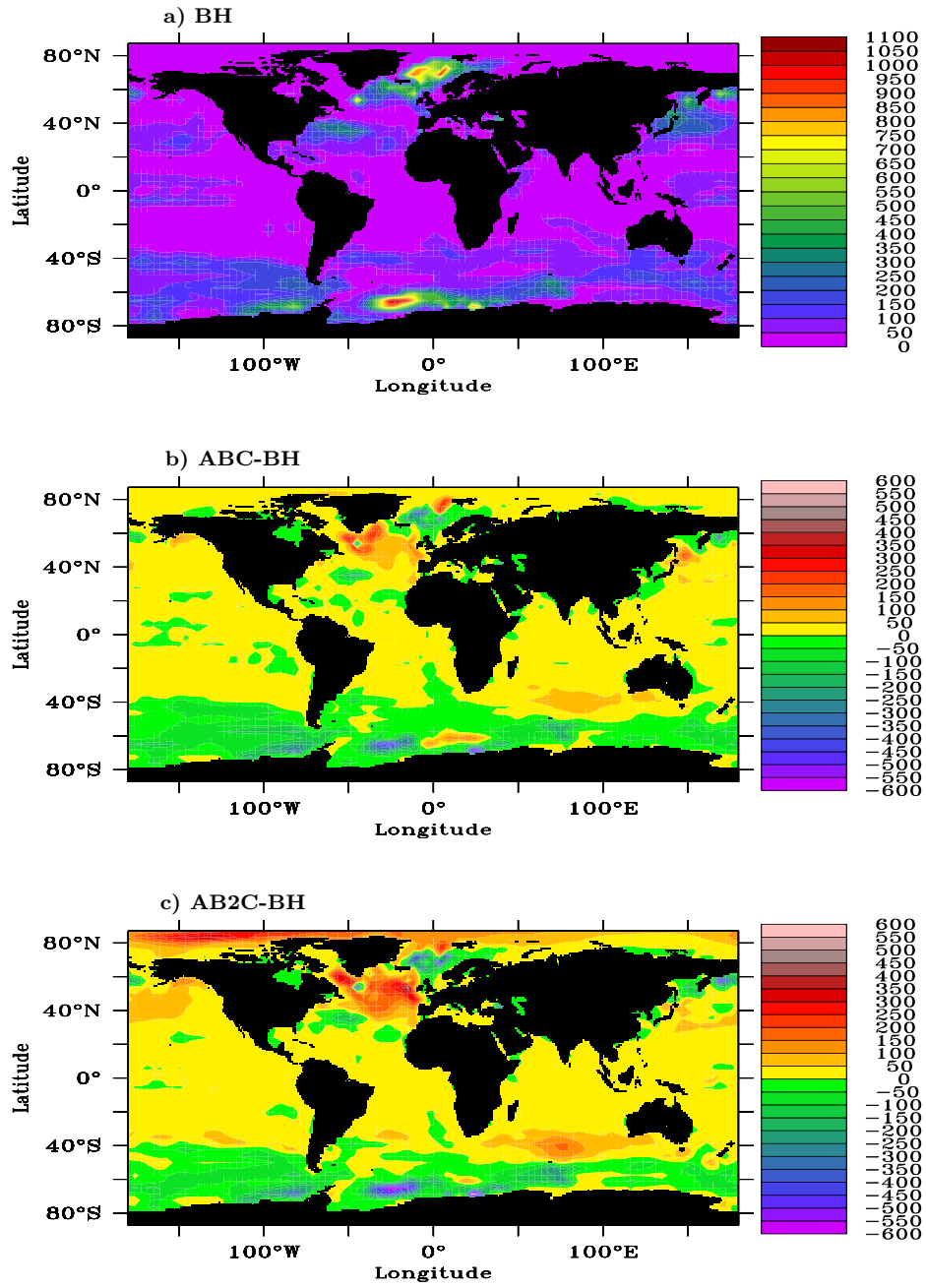


Figure 10: Horizontal distributions of mean convection depth in m for a) the time-mean in experiment BH and b) the difference between experiments ABC and BH and c) between experiments AB2C and BH.

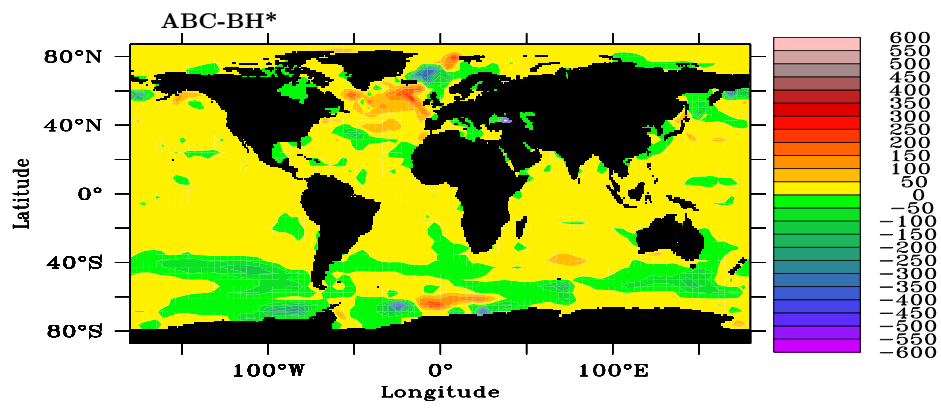


Figure 11: Horizontal distribution of the change in the mean convection depth in m between experiments ABC and BH*.

Table 1: Experiments done with MPI-OM and different versions of EMAD model. $\bar{\mathbf{x}}$ denotes the climatological fluxes and \mathbf{x}' the flux anomalies predicted by different versions of the EMAD model.

name	fluxes used	characteristics
BH	$\bar{\mathbf{x}} + \mathbf{x}'$ $\mathbf{x}'_t = \mathcal{B}\mathbf{y}'_t, (\mathbf{x}' = H', \mathbf{y}' = SST')$	no fluctuations, with SST-feedback on heat flux
ABC	$\bar{\mathbf{x}} + \mathbf{x}',$ $\mathbf{x}'_t = \mathcal{A}\mathbf{x}'_{t-1} + \mathcal{B}\mathbf{y}'_t + \mathcal{C}\mathbf{n}_t$	with fluctuations + feedback
AB2C	$\bar{\mathbf{x}} + \mathbf{x}',$ $\mathbf{x}'_t = \mathcal{A}\mathbf{x}'_{t-1} + \mathcal{B}\mathbf{y}'_t + 2 \times \mathcal{C}\mathbf{n}_t$	with feedback + $2 \times$ fluctuations

Table 2: 200-year means of MOC-index and ACC-index in Sv in different experiments.

Experiment name	MOC-index	ACC-index
BH	17.1	200
ABC	18.3	148
AB2C	21.8	122
ECHAM5/MPI-OM	18.0	186